

# Conductance Switching and Vibrational Fine Structure of a $[2 \times 2]$ $\text{Co}^{\text{II}}_4$ Gridlike Single Molecule Measured in a Three-Terminal Device\*\*

Edgar A. Osorio, Mario Ruben,\* Johannes S. Seldenthuis, Jean-Marie Lehn, and Herre S. J. van der Zant\*

The observation of electrical switching in molecular junctions has recently attracted a lot of attention and the operation of a 160 kB dynamic random access memory (DRAM) circuit based on monolayers of bistable rotaxane molecules as data storage elements has been described.<sup>[1]</sup> Reports on conductance switching in the literature, however, remain controversial with regard to the nature of the mechanism itself: conformational changes,<sup>[2–6]</sup> molecule–bond fluctuations,<sup>[7–9]</sup> or reversible formation of metallic filaments through molecular layers<sup>[10]</sup> are among the proposed mechanisms. Herein, we present a study of conductance switching in molecular junctions carried out using  $[\text{Co}^{\text{II}}_4\text{L}_4](\text{BF}_4)_8$  gridlike  $[2 \times 2]$  molecules in three-terminal devices, where **L** is 4,6-bis(2',2''-bipyrid-6'-yl)-2-phenylpyrimidine). Transport measurements at cryogenic temperatures reveal Coulomb blockade and exhibit excitation lines at low energy, which are attributed to vibrational modes of the molecule. When applying a bias above a threshold voltage, current–voltage ( $I$ – $V$ ) characteristics show switch events between bistable branches. The measurements hint at an electrostatic origin of this effect and we argue that subnanometer motion of electrostatically bound counter ions in the

vicinity of the molecular junction may be the cause, a mechanism so far not yet evoked for positively charged molecules in molecular junctions.<sup>[11,11]</sup>

We have studied three-terminal transport in electro-migrated junctions comprising the  $[\text{Co}^{\text{II}}_4\text{L}_4](\text{BF}_4)_8$  molecular complex. This species consists of an eightfold positively charged cationic  $[\text{Co}^{\text{II}}_4\text{L}_4]^{8+}$  metallosupramolecular core **1** and a cloud of eight compensating single negatively charged  $\text{BF}_4^-$  counter-anions.<sup>[12]</sup> Within the cationic complex moiety the four metal Co(II) ions are positioned by the ligands **L** at the cornerstones of a molecular square (Scheme 1, left and middle). Electrodes with nanometer-scale separation were fabricated by electro-migration<sup>[13]</sup> of a thin gold wire on top of an aluminum gate (see scanning electron microscopy (SEM) image in Scheme 1, right). Complexes were deposited from acetonitrile solution; details of the junction fabrication and characterization are described in the Experimental Section. Transport measurements carried out at cryogenic temperatures reveal clear vibrational spectra as well as, more interestingly, the presence of switching behavior. In this Communication we present the results on three different devices: two showed both vibrational fine structure and switching behavior (samples A and B); a third sample, C, did not display switching events but a set of excitations at comparable energies with samples A and B.

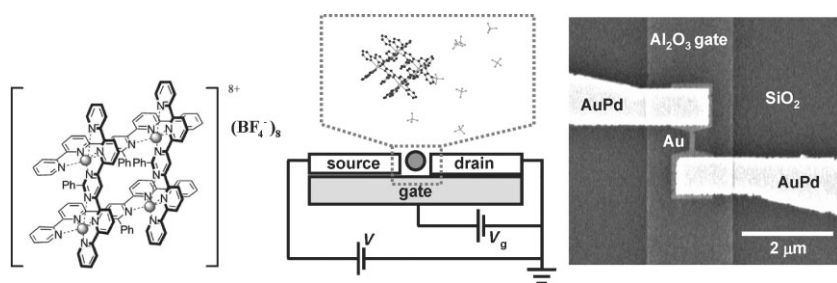
Transport measurements for samples A and B are represented in Figure 1a and b, respectively, as a plot of the differential conductance as a function of bias and gate voltage. Regions of high conductance (white and gray), where transport takes place through sequential electron tunneling (SET), are separated by slanted lines (diamond edges) from regions of zero conductance (black), which is a signature of Coulomb blockade physics. For samples A and B, only two charge states are probed in the experiment, which we label N and N + 1. We observe in both transport measurements sharp spectroscopic features, that is, excitation lines, in the SET region, indicating a weak (electronic) molecule–lead coupling. We have included the energies of these excitations in Table 1 for samples A and B for the two consecutive charge states; for energies above 10 meV, other sets of measurements, not shown here, were used to determine these. We have also included the energy of the excitations for sample C, which also displayed only two charge states. From Table 1, it appears that the three samples share excitations at comparable energies. The fact that

[\*] Prof. H. S. J. van der Zant, Dr. E. A. Osorio, J. S. Seldenthuis  
Kavli Institute of Nanoscience  
Delft University of Technology  
PO Box 5046, 2600 GA, Delft (The Netherlands)  
E-mail: h.s.j.vanderZant@tudelft.nl

Dr. M. Ruben, Prof. J.-M. Lehn  
Karlsruhe Institute of Technology (KIT)  
Institut für Nanotechnologie  
Postfach 3640, 76021 Karlsruhe (Germany)  
E-mail: mario.ruben@int.fzk.de

Prof. J.-M. Lehn  
ISIS, Université de Strasbourg  
8, Allée Gaspard Monge  
BP 70028, F-67083 Strasbourg (France)

[\*\*] We thank Kevin O'Neill for the work on electromigration, and Maarten Wegewijs and Jos Thijssen for useful discussions. Financial support was obtained from the Dutch Organization for Fundamental Research on Matter (FOM), the Nederlandse Organisatie voor Wetenschappelijk Onderzoek (NWO), the EU FP7 programme under the grant agreement SINGLE, and the Deutsche Forschungsgemeinschaft (DFG) within the Priority Program Quantrans.



**Scheme 1.** Schematic representation of the [Co<sub>4</sub><sup>II</sup> L<sub>4</sub>](BF<sub>4</sub><sup>-</sup>)<sub>8</sub> complex (left) and the device lay-out with the molecular structure derived from X-ray analysis data (middle).<sup>[11c]</sup> The Co<sup>II</sup> centers are held by four ligands **L** in square positions and each complex cation [Co<sub>4</sub><sup>II</sup> L<sub>4</sub>]<sup>8+</sup> is surrounded by a cloud of eight negatively charged BF<sub>4</sub><sup>-</sup> counter anions. Right) SEM image of a fabricated device prior to breaking the faint small gold wire in the middle by electromigration.

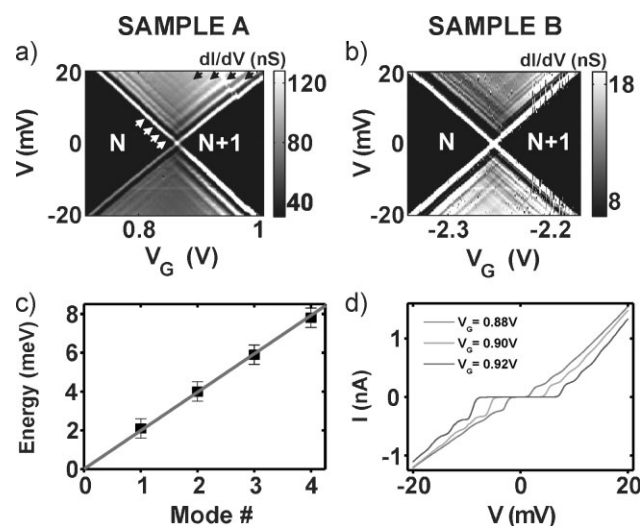


**Figure 1.** a,b) Conductance maps of two different junctions (samples A and B) incorporating a grid-type complex in the weak coupling limit measured at 1.6 K, and with a maximum applied bias voltage of  $\pm 20$  mV. The gate coupling is deduced from the slopes of the diamond edges and equals  $\beta_A = 0.1$  and  $\beta_B = 0.12$  for samples A and B, respectively. c) Energy of the first four vibrational excitations in charge state *N* as a function of the mode number (sample A). d) *I*-*V* characteristics at three different gate voltages from the measurement in (a) showing a step-wise increase of the current due to the excitation of the *n*<sup>th</sup> vibrational mode (squares in (c)).

some excitations are absent (present) for one sample and not for the other may hint at a difference in electron-phonon coupling, which could be related to a difference in the environment for the molecule in the three devices, or different molecule-lead couplings.<sup>[14]</sup>

It is important to remark that given the energy spacing of the excitations (few meV) and their appearance at approximately the same energies for two subsequent charge states, they originate from vibrational modes.<sup>[15]</sup> Further confirmation comes from the observation of four harmonic excitation lines indicated in Figure 1a by arrows; in Figure 1c we have plotted the energy of these four excitations as a function of the mode number and in Figure 1d the corresponding *I*-*V* characteristics. Such a harmonic spectrum indicates excitation of four

vibrational quanta with an electron-phonon coupling of the order one.<sup>[16,17]</sup> From the step heights in Figure 1d, an estimate of the electron-phonon coupling constant,  $\lambda$ , can be obtained. In the approximation that transitions involve at least one ground state, one finds that the ratio between the second and first step height equals  $\lambda$ .<sup>[16,17]</sup> In Figure 1d this ratio is close to one for all three curves; thus, the data indicates  $\lambda \approx 1$ . To get more insight in the nature of the vibrational modes and their appearance in an experiment, quantum chemistry calculations would be helpful. However, at low energies the calculations are very sensitive to the local environment

(potential landscape) and this may make it difficult to identify the exact mode that appears in the experiment.

Transport measurements in sample A were carried out on a larger bias and gate range. In Figure 2a we show the conductance map acquired with a maximum applied bias of  $\pm 200$  mV. A striking difference with Figure 1a is observed: the stability diagram no longer shows a clearly defined degeneracy point at  $V_G = 0.8$  V. Diamond edges are ill defined as the onset of conductance appears to be stochastically distributed (switching behavior) for every gate voltage. In addition, a pronounced negative differential resistance (NDR) region (black) appears at positive bias. Figure 2b shows an expanded view on the central region of the stability diagram, which shows the switching behavior in more detail. As a guide and for the purpose of the upcoming discussion, we have added

**Table 1.** Energy of the excitations lines (in meV) listed for two consecutive charge states probed in the experiment (for samples A, B, and C). These are read from the bias at which the excitation line meets the diamond edge; the excitation corresponds to the charge state of the Coulomb diamond they end up in. The error in the reading is about 0.5 meV.

Sample A		Sample B		Sample C	
N	N + 1	N'	N' + 1	N''	N'' + 1
	1.1	1.1	1.2		
2.1	2.1	1.9	1.5		
	3.5	2.6	2.3	2.8	2.6
4		3.2	3.2		
		3.8	4.0	3.8	3.9
			4.4		
	5.1	4.7	4.9	5.0	4.9
5.9	6.2	5.6	5.7	6.1	6.1
		6.4	6.0		
			6.8		
7.8	7.6	7.3	7.6	7.0	7.8
		8.5	8.5		
		9.9	9.0		9.1
		10.7	10.2	10.2	10.5
		12	11.9		
		14.3	13.8	13.1	14.2
		17.5	17.2	16.0	17.1
		20.7	20.1	20.0	20.4
		24	23.6	23	23.4
		27.0	26.6	26.6	27.1
		30		30	
48	44				

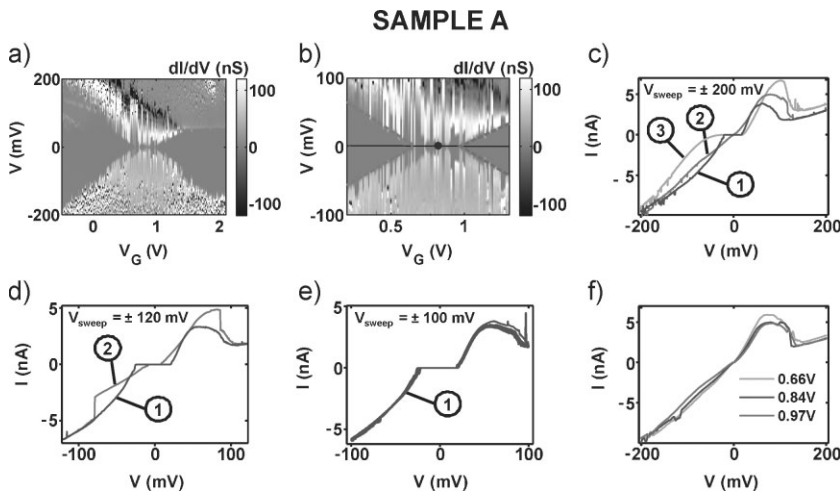


**Figure 2.** a) Conductance map of sample A measured at 1.6 K with a maximum applied bias of  $\pm 200$  mV. b) Zoom-in of the central region in the stability diagram shown in (a). c–e) Recorded  $I$ – $V$  curves taken by sweeping the bias voltage back and forth continuously between  $\pm 200$  mV,  $\pm 120$  mV, and  $\pm 100$  mV at  $V_G = 1$  V. For clarity, a limited number of curves is shown in each panel; numbers label each type of characteristic  $I$ – $V$ . f)  $I$ – $V$  curves taken from (a) at  $V_G = 0.66$  V, 0.84 V, and 0.97 V.

green and red dashed lines in Figure 2b, which represent a lower-bias bound for the onset of conductance.

To study this stochastic behavior in more detail we continuously measured  $I$ – $V$  characteristics at  $V_G = 1$  V from  $-200$  mV to  $+200$  mV and back. We acquired 200 of these sweeps, and in Figure 2c we have plotted three  $I$ – $V$  curves, which are representative of the overall behavior during these measurements. A common feature of all three curves is the broad NDR located at positive bias. Apart from having slightly different current levels, the three curves display a different Coulomb gap size: curve 2 (curve 3) is the one with the smallest (largest) gap in Figure 2c. We also note that curve 3 has a less sharp onset of conductance as compared to curve 1: this is clearer at negative bias. It is important to note that during the 200 sweeps, stochastic switching between the different  $I$ – $V$  curves is observed for biases higher than  $\pm 80$  mV. This is marked by vertical transitions in the  $I$ – $V$  characteristic, as observed in Figure 2c at approximately  $-200$  mV in bias.

By decreasing the maximum applied bias in the sweeps, we find that it has a profound influence on the switching. In Figure 2d we show two representative  $I$ – $V$  characteristics in which the bias voltage of the sweeps was limited to  $\pm 120$  mV. Compared to the previous measurement in which the bias was limited to  $\pm 200$  mV, we did not observe in a total of 200 sweeps the curve 3-type  $I$ – $V$  characteristic as shown in Figure 2c; all recorded  $I$ – $V$  curves were similar to those in Figure 2d. We also note that stochastic switching between  $I$ – $V$  types is observed, and in Figure 2d we see a clear transition from curve 2 to curve 1 type at approximately  $-80$  mV. Below a threshold bias voltage in the sweeps,  $V \approx 100$  mV, the switching between different types of  $I$ – $V$  curve completely disappears. In Figure 2e we show 20 out of 200 consecutive sweeps performed with a maximum applied voltage of  $\pm 100$  mV. It is clear that curve 1 type of  $I$ – $V$  characteristic remains.

The stability of the  $I$ – $V$  characteristic below this voltage explains why in Figure 1a, where the applied bias did not exceed 20 mV, well-defined diamond edges are observed. In addition, the position in gate voltage of the charge degeneracy point in Figure 1a coincides with the position of the central dot in Figure 2b. Close inspection of Figure 2b shows that the charge degeneracy point shifts between three different fixed positions at the gate axis. To illustrate this point, in Figure 2f we present  $I$ – $V$  characteristics at three different gate voltages: at each of the crossings defined by the dashed lines and at the position of the central dot in Figure 2b. We see that all three curves are similar and share the absence of a clear conductance gap, confirming our observations. The separation in gate voltage between these three curves is about 0.11 V, which, multiplied by the experimentally determined gate coupling  $\beta_A (=0.1)$ , gives a separation in energy of about  $\Delta_A = 11$  meV.

We have observed a similar switching effect for sample B. Figure 3a shows the conductance map and, as for sample A, we see that well-defined diamond edges are absent as the onset of conductance is no longer linear on  $V_G$  (see Figure 3b). With dashed we highlight in Figure 3a two possible onsets of conductance, which are connected to two different charge degeneracy points of the same state separated in gate voltage by 0.12 V or in energy by  $\Delta_B = 15$  meV, with the experimentally determined  $\beta_B = 0.12$  (the crossing point of the dashed lines defines these two points).

In the same manner as for sample A, we have measured at a fixed gate voltage  $I$ – $V$  characteristics from  $-200$  mV to  $+200$  mV and back. By measuring continuously 300 of these sweeps, we found that two representative  $I$ – $V$  characteristics appear (plotted in Figure 3b). We note that in Figure 3b curve 2 switches at positive and negative bias voltages (indicated by arrows) to curve 1. In Figure 3c we have plotted 100 consecutive sweeps. We observe a frequent stochastic switching between the two  $I$ – $V$  curves. The current levels are practically the same for all sweeps and the main difference between the two curves is the conductance gap size: it is smaller for curve 1. The size of the conductance gap for curve 2 (curve 1) is equal to the gap size that one would determine from each of the two possible diamond edges schematically drawn in Figure 3a with dashed lines. As with sample A, below a certain threshold bias voltage (about 50 mV in this case), sample B stops displaying switching between different  $I$ – $V$  curves. In Figure 3d we show 20 out of 300 consecutive sweeps with a maximum applied bias voltage of 50 mV: only curve 1 is recorded. For the measurement presented in Figure 1b the bias was kept below this threshold value. We note that the leftmost crossing defined by the dashed lines in Figure 3a is located at the same gate voltage as the degeneracy point in Figure 1b.

Based on the observations, we can disregard a number of mechanisms that may induce the switching behavior. First of all,

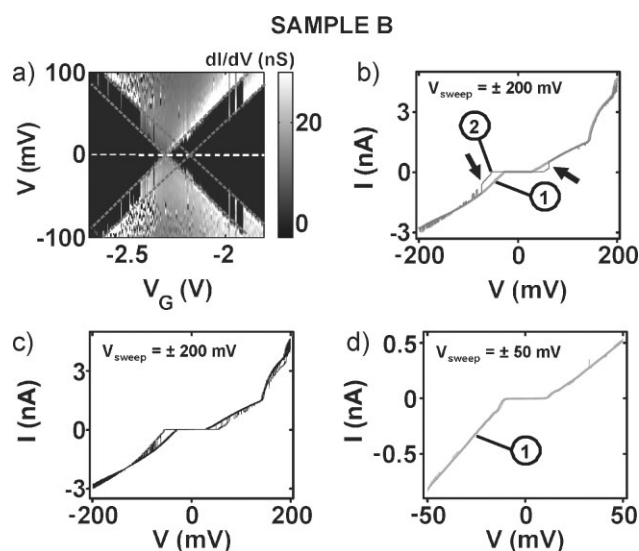


**Figure 3.** a) Conductance map of sample B measured at 1.6 K, and with a maximum applied bias of  $\pm 200$  mV (shown data was truncated between  $\pm 100$  mV for clarity). b, c) Recorded  $I$ - $V$  curves taken by sweeping the bias voltage back and forth continuously between  $\pm 200$  mV at  $V_G = -2.4$  V. In (b) and (c), 2 and 100  $I$ - $V$  curves are shown, respectively. Arrows in (b) point at a transition between characteristic  $I$ - $V$  curves (see text). d) Same as (c) but for a limiting bias of  $\pm 50$  mV. A total of 20 sweeps is displayed.

molecule–Au bond fluctuations cannot explain the observed switching since the grid molecule does not possess attaching linker groups (such as S–H). In contrast, fixation of  $[\text{Co}^{\text{II}}_4\text{L}_4]$  ( $\text{BF}_4$ )<sub>8</sub> in the nanogap is thought to happen by partial electrostatic screening of the positively charged complex moiety by the electron density on the metallic Au electrodes. Moreover, for large molecules conformational changes are not likely to be the cause as they are only expected to change the  $I$ - $V$  characteristic above a certain bias voltage and not the conductance gap. Claims of the observation of conformational changes have been reported with scanning tunneling microscopy (STM) experiments. In these experiments the zero-bias resistance and the low-bias behavior remained unchanged,<sup>[4,5]</sup> in contrast to our observations.

The fact the charge degeneracy point is stochastically shifting suggests that the switching effect is electrostatic in nature. Charges near the molecular junctions might be the cause. The  $[\text{Co}^{\text{II}}_4\text{L}_4]^{8+}$  grid complex has an intrinsic charge of plus eight. Neighboring complexes that do not contribute to transport could have an electrostatic influence on the conducting molecule. Furthermore, the solutions that are used for the deposition of these molecules contain counter ions (molecular species that ensure charge neutrality of the whole compound). After deposition these negatively charged, spatially highly flexible counter anions may remain in the vicinity of the junction area; by moving around they mimic a change in the offset charge, which leads to a shift of the degeneracy point.

In order to gain further insight into this scenario we have carried out both *ab initio* quantum chemistry calculations, and calculations based on solving Poisson's equation for the

junction in the presence of the eight  $\text{BF}_4^-$  counter ions (see Supporting Information for details). Both methods indicate that a counter ion displacement of about half an Ångström (approximately half of the diameter of the counter ion) induces a potential change on the molecule comparable to the experimental value ( $\Delta_A = 11$  meV;  $\Delta_B = 15$  meV). This suggests that even a partial rotation of a single counter ion would be enough to induce the switching effect. We note that the interpretation of counter ion motion (e.g., rotation) is consistent with the observation of a threshold bias voltage since a potential energy barrier is expected for such a displacement.

In other systems such as semiconducting quantum dots,<sup>[18]</sup> silicon nanowires,<sup>[19]</sup> and single-electron transistors (SETs)<sup>[20,21]</sup> charge traps have been indentified as the cause of switching events. Thus, we have considered as another possible scenario for the switching behavior in our junctions the presence of a charge trap in the gate oxide. Our calculations indicate that if a charge trap is located approximately one nanometer below the oxide surface, the charging of the trap with one electron could induce the required potential change ( $\approx 10$  meV) on the molecule. However, we find that this scenario is unlikely, and the reasoning goes as follows. The experiments show that switching occurs when the bias voltage exceeds  $\approx 100$  mV; this value corresponds to a calculated potential change at the location of the charge trap of about 20 mV. On the other hand, we have determined that a change in gate voltage of 100 mV induces a potential variation at the charge trap of about 50 mV; the gate coupling for the charge trap is large,  $\approx 0.5$ . Hence, if the bias voltage can charge the trap, the gate voltage should also do so, even at low bias. In Figure 1a (b), switching is not observed over a gate voltage range larger than 200 mV (100 mV).

It is also important to note that we have never observed a similar switching behavior in measurements carried out on the oligophenylenevinylene (OPV) molecules<sup>[15,22]</sup> or in the sulfur end-functionalized teracyclohexylidenes (3R) molecules, which do not have counter ions.<sup>[23]</sup> In 10 out of 415 and in 17 out of 449 measured junctions, transport was attributed to transport through single OPV-5 and 3R molecules, respectively. In none of these 10 (17) junctions was switching behavior observed. Since the device fabrication has been the same for these junctions, this observation further corroborates our conclusion that the switching behavior we report here is due to the presence of counter ions.

Since the multitude of metal complexes owning interesting electronic, magnetic, or photophysical properties are designed by charged molecule moieties, the results presented herein show clearly that electrostatically bound counter anions have a significant influence on the transport properties, even inducing switching regimes in transport, and their presence can not be ignored. This is a result of general importance for the design and implementation of highly integrated molecular electronic (and spintronic) devices comprising charged molecules as active units in its architecture.<sup>[1,3,11]</sup> In order to gain further insight into the origin of the observed switching effects, it would be of interest to investigate, for instance, the following three types of system: 1) The same grid-type species **1**, synthesized with significantly different counter anions; 2) species of type **1** based

on ligands bearing negatively charged groups directly linked to the ligand molecule and thus unable to move around; 3) neutral analogs of **1** obtained by using ligands containing ionizable groups, such as hydrazones.<sup>[24]</sup>

### Experimental Section

The complex  $[\text{Co}^{\text{II}}_4\text{L}_4](\text{BF}_4)_8$  was obtained following a synthetic protocol reported previously.<sup>[12]</sup> Electrodes with nanometer separation were fabricated by electromigration. Briefly, we prepared a 10-nm-thick gold wire (width 100 nm, length 500 nm) on top of an Al/Al<sub>2</sub>O<sub>3</sub> gate electrode using e-beam lithography (Scheme 1). The aluminum was oxidized in air, forming a 2- to 4-nm-thick Al<sub>2</sub>O<sub>3</sub> layer which, at low temperatures, started to show leakage currents for voltages above  $\pm 4$  V. AuPd leads, 100 nm thick, were used to contact the thin gold bridge. To create a nanogap, electromigration was performed using an active breaking scheme, similar to those previously reported.<sup>[25]</sup> With this method, nanoconstrictions with a resistance in the k $\Omega$  range can be achieved with high reproducibility.

For the deposition of a molecule in the junction we used a home-made liquid cell, placed inside a <sup>4</sup>He cryostat, containing a 0.1 mM molecule solution. At room temperature, electromigration was performed in a liquid environment on about 16 junctions that were rinsed with the pure solvent, dried, and cleaned in an oxygen plasma beforehand. Nanoconstrictions with a resistance in the k $\Omega$  range were first prepared in the solution containing the molecules. The electromigrated junctions were then left in the molecule solution for about half an hour to allow for “self-breaking”<sup>[26]</sup> of the constricted gold wire. Junctions that did not self-break within this time were then deliberately broken at conductances higher than  $G_0$ . Lastly, the sample space was evacuated and the cooling procedure to 1.7 K began. In total, 100 junctions were measured.

### Keywords:

molecular junctions · offset charges · switching · three-terminal devices · vibrational modes

- [1] J. E. Green, J. Wook Choi, A. Boukai, Y. Bunimovich, E. Johnston-Halperin, E. Delonno, Y. Luo, B. A. Sheriff, K. Xu, Y. Shik Shin, H. R. Tseng, J. F. Stoddart, J. R. Heath, *Nature* **2007**, *445*, 414–417.
- [2] J. Gaudioso, L. J. Lauhon, W. Ho, *Phys. Rev. Lett.* **2000**, *85*, 1918–1921.
- [3] E. Lortscher, J. Ciszek, J. Tour, H. Riel, *Small* **2006**, *2*, 973–977; M. Ruben, A. Landa, E. Lortscher, H. Riel, M. Mayor, H. Gorls, H. B. Weber, A. Arnold, F. Evers, *Small* **2008**, *4*, 2229–2235.

- [4] B.-Y. Choi, S.-J. Kahng, S. Kim, H. Kim, H. W. Kim, Y. J. Song, J. Ihm, Y. Kuk, *Phys. Rev. Lett.* **2006**, *96*, 156106.
- [5] X. H. Qiu, G. V. Nazin, W. Ho, *Phys. Rev. Lett.* **2004**, *93*, 196806.
- [6] A. V. Danilov, P. Hedegård, D. S. Golubev, T. Bjørnholm, S. E. Kubatkin, *Nano Lett.* **2008**, *8*, 2393–2398.
- [7] G. K. Ramachandran, T. J. Hopson, A. M. Rawlett, L. A. Nagahara, A. Primak, S. M. Lindsay, *Science* **2003**, *300*, 1413–1416.
- [8] A. V. Danilov, S. E. Kubatkin, S. G. Kafanov, K. Flensberg, T. Bjørnholm, *Nano Lett.* **2006**, *6*, 2184–2190.
- [9] E. Lortscher, H. B. Weber, H. Riel, *Phys. Rev. Lett.* **2007**, *98*, 176807.
- [10] C. N. Lau, D. R. Stewart, R. S. Williams, M. Bockrath, *Nano Lett.* **2004**, *4*, 569–572.
- [11] J. Park, A. N. Paspapathy, J. I. Goldsmith, C. Chang, Y. Yalsh, J. R. Petta, M. Rinkoski, J. P. Sethna, H. D. Abruña, P. L. McEuen, D. C. Ralph, *Nature* **2002**, *417*, 722.
- [12] a) M. Ruben, E. Breuning, J.-P. Giesselbrecht, J.-M. Lehn, *Angew. Chem. Int. Ed.* **2000**, *39*, 4139–4142; b) M. Ruben, E. Breuning, M. Barboiu, J. P. Giesselbrecht, J. M. Lehn, *Chem. Eur. J.* **2003**, *9*, 291–299; c) J. Rojo, F. Romero-Salguero, J.-M. Lehn, G. Baum, D. Fenske, *Eur. J. Inorg. Chem.* **1999**, *1999*, 1421–1428.
- [13] H. Park, A. K. L. Lim, A. P. Alivisatos, J. Park, P. L. McEuen, *Appl. Phys. Lett.* **1999**, *75*, 301–303.
- [14] N. P. de Leon, W. Liang, Q. Gu, H. Park, *Nano Lett.* **2008**, *8*, 2963–2967.
- [15] E. A. Osorio, K. O'Neill, N. Stuhr-Hansen, O. F. Nielsen, T. Bjørnholm, H. S. J. van der Zant, *Adv. Mater.* **2007**, *19*, 281.
- [16] H. Park, J. Park, A. K. L. Lim, E. H. Anderson, A. P. Alivisatos, P. L. McEuen, *Nature* **2000**, *407*, 57–60.
- [17] S. Braig, K. Flensberg, *Phys. Rev. B.* **2003**, *68*, 205324.
- [18] S. W. Jung, T. Fujisawa, Y. Hirayama, Y. H. Jeong, *Appl. Phys. Lett.* **2004**, *85*, 768.
- [19] M. Hofheinz, X. Jehl, M. Sanquer, G. Molas, M. Vinet, S. Deleonibus, *Eur. Phys. J. B* **2006**, *54*, 299.
- [20] N. M. Zimmerman, J. L. Cobb, A. F. Clark, *Phys. Rev. B.* **1997**, *56*, 7675.
- [21] D. E., Grupp, T. Zhang, G. J. Dolan, N. S. Wingreen, *Phys. Rev. Lett.* **2001**, *87*, 186805.
- [22] E. A. Osorio, K. O'Neill, M. Wegewijs, N. Stuhr-Hansen, J. Paaske, T. Bjørnholm, H. S. J. van der Zant, *Nano Lett.* **2007**, *7*, 3336.
- [23] M. Poot, E. Osorio, K. O'Neill, J. M. Thijssen, D. Vanmaekelbergh, C. A. van Walree, L. W. Jenneskens, H. S. J. van der Zant, *Nano Lett.* **2006**, *6*, 1031.
- [24] M. Ruben, J.-M. Lehn, G. Vaughan, *Chem. Comm.* **2003**, 1338–1339.
- [25] D. R. Strachan, D. E. Smith, D. E. Johnston, T.-H. Park, M. J. Therien, D. A. Bonnell, A. T. Johnson, *Appl. Phys. Lett.* **2005**, *86*, 043109.
- [26] K. O'Neill, E. A. Osorio, H. S. J. van der Zant, *Appl. Phys. Lett.* **2007**, *90*, 133109.

Received: August 20, 2009

Revised: October 14, 2009

Published online: November 26, 2009